Optical trapping of director structures and defects in liquid crystals using laser tweezers

Ivan I. Smalyukh[1, 2*], Daniel S. Kaputa[1], Aliaksandr V. Kachynski[1], Andrey N. Kuzmin[1], and Paras N. Prasad[1]

[1]*The Institute for Lasers, Photonics, and Biophotonics, University at Buffalo, The State University of New York, Buffalo, New York 14260-3000*

[2]*Department of Materials Science and Engineering, University of Illinois at Urbana-Champaign, Illinois 61801*

* *smalyukh*@uiuc.edu

Abstract: We demonstrate optical manipulation of structures and defects in liquid crystals (LCs). The effective refractive index depends on the LC molecular orientations and the laser beam's polarization. We use the orientation-mediated refractive index contrast for the laser trapping in LCs with a homogeneous composition, but with spatially-varying patterns of molecular orientations. Tightly-focused polarized beams allow for optical trapping of disclinations and their clusters, dislocations and oily streaks, cholesteric fingers and focal conic domains, etc. We calculate the optical gradient forces for typical structures and explain the trapping properties at low laser powers. We also show that when a high-power beam causes local molecular realignment, the laser trapping properties change for two reasons: (1) the refractive index pattern and optical gradient forces are modified; (2) additional elastic structural forces arise to minimize the elastic free energy.

OCIS codes: (160.1190) Anisotropic optical materials; (140.7010) Laser Trapping; (160.3710) Liquid crystals; (180.6900) Three-dimensional microscopy; (260-1440) Birefringence.

References and links

1. A. Ashkin, J. M. Dziedzic, J. E. Bjorkholm, and S. Chu, "Observation of a single-beam gradient force optical trap for dielectric particles," Opt. Lett. **11**, 288 (1986).
2. P. N. Prasad, *Introduction to Biophotonics* (Wiley, New York, 2003).
3. K. C. Neuman and S. M. Block, "Optical trapping," Rev. Sci. Instrum. **75**, 2787 (2004).
4. D. G. Grier, "A revolution in optical manipulation," Nature **424**, 810 (2003).
5. Y. Roichman and D. G. Grier, "Holographic assembly of quasicrystalline photonic heterostructures," Opt. Express **13**, 5434 (2005).
6. T. A. Wood, H. F. Gleeson, M. R. Dickinson, and A. J. Wright , "Mechanisms of optical angular momentum transfer to nematic liquid crystalline droplets," Appl. Phys. Lett. **84**, 4292 (2004).
7. I. I. Smalyukh, O. D. Lavrentovich, A. Kuzmin, A. Kachynski, and P. N. Prasad, "Elasticity-mediated self-organization and colloidal interactions of solid spheres with tangential anchoring in a nematic liquid crystal," Phys. Rev. Lett. **95**, 157801 (2005).
8. M. Yada, J. Yamamoto, and H. Yokoyama, "Direct observation of anisotropic interparticle forces in nematic colloids with optical tweezers," Phys. Rev. Lett. **92**, 185501 (2004).
9. A. Pattanaporkratana, C. S. Park, J. E. Maclennan, and N. A. Clark, "Manipulation of disk-shaped islands on freely suspended smectic films and CDs using optical tweezers," Ferroelectrics **310**, 131 (2004).
10. I. I. Smalyukh, A. Kuzmin, A. Kachynski, P. N. Prasad, and O. D. Lavrentovich, "Optical trapping of colloidal particles and measurement of the defect line tension and colloidal forces in a thermotropic nematic liquid crystal," Appl. Phys. Lett. **86**, 021913 (2005).
11. M. Škarabot, M. Ravnik, D. Babič, N. Osterman, I. Poberaj, S. Žumer, I. Muševič, A. Nych, U. Ognysta, and V. Nazarenko, "Laser trapping of low refractive index colloids in a nematic liquid crystal," Phys. Rev. E **73**, 021705 (2006).
12. I. Muševič, M. Škarabot, D. Babič, N. Osterman, I. Poberaj, V. Nazarenko, A. Nych, "Laser trapping of small colloidal particles in a nematic liquid crystal: clouds and ghosts," Phys. Rev. Lett. **93**, 187801 (2004).
13. I. I. Smalyukh, B. I. Senyuk, S. V. Shiyanovskii, O. D. Lavrentovich, A. N. Kuzmin, A. V. Kachynski, and P. N. Prasad, "Optical trapping, manipulation, and 3-D Imaging of disclinations in liquid crystals and measurement of their line tension," Mol. Cryst. Liq. Cryst. **450**, 79 (2006).

#78218 - $15.00 USD Received 21 December 2006; revised 25 February 2007; accepted 26 February 2007

14. I. I. Smalyukh, A. V. Kachynski, A. N. Kuzmin, and P. N. Prasad, "Laser trapping in anisotropic fluids and polarization controlled particle dynamics," Proc. Natl. Acad. Sci. U.S.A. **103**, 18048 (2006).
15. S. Juodkazis, M. Shikata, T. Takahashi, S. Matsuo, and H. Misawa, "Fast optical switching by a laser-manipulated micro-droplet of liquid crystal," Appl. Phys. Lett. **74**, 3627 (1999).
16. S. Juodkazis, S. Matsuo, N. Murazawa, I. Hasegawa, and H. Misawa, "High-efficiency optical transfer of torque to a nematic liquid crystal droplet," Appl. Phys. Lett. **82**, 4657 (2003).
17. P.-G. de Gennes and J. Prost, *The Physics of Liquid Crystals* (Clarendon, Oxford, 1993), 2nd Ed.
18. P. M. Chaikin and T. C. Lubensky, *Principles of Condensed Matter Physics*, (Cambridge University Press, Cambridge, 1995).
19. E. Hatta and Th. M. Fischer, "Liquid crystalline and solid stripe textures in Langmuir monolayers," Langmuir **18**, 6201 (2002).
20. S. Wurlitzer, P. Steffen and Th. M. Fischer, "Line tension of Langmuir monolayer phase boundaries determined with optical tweezers," J. Chem. Phys. **112**, 5915 (2000).
21. S. Wurlitzer, P. Steffen, M. Wurlitzer, Z. Khattari, and Th. M. Fischer, "Line tension in Langmuir monolayers probed by point forces" J. Chem. Phys. **113**, 3822 (2000).
22. P. Steffen, S. Wurlitzer, and Th. M. Fischer, "Hydrodynamics of shape relaxation in viscous Langmuir monolayer domains" J. Phys. Chem. A **105**, 8281 (2001).
23. S. Wurlitzer, C. Lautz, M. Liley, C. Duschl, and Th. M. Fischer, "Micromanipulation of Langmuir monolayers with optical tweezers" J. Phys. Chem. B **105**, 182 (2001).
24. E. Hatta and Th. M. Fischer, "Splitting of an s = 1 point disclination into half-integer disclinations upon laser heating of a Langmuir monolayer," J. Phys. Chem. B **107**, 6406 (2003).
25. J. Hotta, K. Sasaki, and H. Masuhara, "Manipulation of liquid crystal textures with a focused near infrared beam," Appl. Phys. Lett. **71**, 2085 (1997).
26. N. Murazawa, S. Juodkazis, and H. Misawa, "Laser manipulation of a smectic liquid-crystal droplet," Euro. Phys. J. E **20**, 435 (2006).
27. N. Murazawa, S. Juodkazis, and H. Misawa, "Laser manipulation based on a light-induced molecular reordering," Opt. Express **14**, 2481 (2006).
28. N. Murazawa, S. Juodkazis, V. Jarutis, Y. Tanamura, and H. Misawa, "Viscosity measurement using a rotating laser-trapped microsphere of liquid crystal," Europhys. Lett. **73**, 800 (2006).
29. N. Murazawa, S. Juodkazis, S. Matsuo, and H. Misawa, "Control of the molecular alignment inside liquid-crystal droplets by use of laser tweezers," Small **1**, 656 (2005).
30. A. Fernández-Nieves, G. Cristobal, V. Garcés-Chávez, G. C. Spalding, K. Dholakia, and D. A. Weitz, "Optically anisotropic colloids of controllable shape," Adv. Mater. **17**, 680 (2005).
31. T. Tlusty, A. Meller, and R. Bar-Ziv, "Optical gradient forces of strongly localized fields," Phys. Rev. Lett. **81**, 1738 (1998).
32. I. I. Smalyukh and O. D. Lavrentovich, Three-dimensional director structures of defects in Grandjean-Cano wedges of cholesteric liquid crystals studied by fluorescence confocal polarizing microscopy," Phys. Rev. E **66**, 051703 (2002).
33. I. I. Smalyukh and O. D. Lavrentovich, "Anchoring-mediated interaction of edge dislocations with bounding surfaces in confined cholesteric liquid crystals," Phys. Rev. Lett. **90**, 085503 (2003).
34. I. I. Smalyukh, B. I. Senyuk, P. Palffy-Muhoray, O. D. Lavrentovich, H. Huang, E. C. Gartland, Jr., V. H. Bodnar, T. Kosa, and B. Taheri, "Electric-field-induced nematic-cholesteric transition and three-dimensional director structures in homeotropic cells," Phys. Rev. E **72**, 061707 (2005).
35. I. I. Smalyukh, S. V. Shiyanovskii, and O. D. Lavrentovich,"Three-dimensional imaging of orientational order by fluorescence confocal polarizing microscopy," Chem. Phys. Lett. **336**, 88 (2001).
36. I. I. Smalyukh, R. Pratibha, N. V. Madhusudana, and O. D. Lavrentovich, "Selective imaging of 3-D director fields and study of defects in biaxial smectic A liquid crystals," Eur. Phys. J. E **16**, 179 (2005).
37. D. S. Kaputa, A. N. Kuzmin, A. V. Kachynski, A. N. Cartwright, P. N. Prasad, "Dynamics of multiple particle trapping by a single beam laser tweezer," Appl. Opt. **44**, 3963 (2005).
38. B. Richards and E. Wolf, "Electromagnetic diffraction in optical systems II. Structure of the image field in an aplanatic system," Proc. R. Soc. London, Ser. A **253**, 358 (1959).
39. A. Rohrbach, "Stiffness of optical traps: quantitative agreement between experiment and electromagnetic theory, "Phys. Rev. Lett. **95**, 168102 (2005).
40. S. D. Durbin, S. M. Arakelian, and Y. R. Shen, "Optical-field-induced birefringence and Freedericksz transition in a nematic liquid crystal," Phys. Rev. Lett. **47**, 1411 (1981).
41. E. Santamato, G. Abbate, P. Maddalena, and Y. R. Shen, "Optically induced twist Freedericksz transition in planar-aligned nematic liquid crystals," Phys. Rev. A **36**, 2389 (1987).
42. I.-C. Khoo, *Liquid Crystals: Physical Properties and Nonlinear Optical Phenomena* (Wiley, New York, 1995).
43. I.-C. Khoo, P. Y. Yan, and T. H. Liu, "Nonlinear transverse dependence of optically induced director axis reorientation of a nematic liquid crystal film - theory and experiment," J. Opt. Soc. Am. B **4**, 115 (1987).
44. E. J. G. Peterman, F. Gittes, and C. F. Schmidt, "Laser-induced heating in optical traps," Biophys. J. **84**, 1308 (2003).

#78218 - $15.00 USD Received 21 December 2006; revised 25 February 2007; accepted 26 February 2007

1. Introduction

Optical trapping with tightly focused laser beams has been broadly applied to objects as diverse as biological molecules, colloidal particles, and living cells [1-3]. The manipulation of multiple objects has been demonstrated by the use of holographic tweezers and time-shared trapping [2-5]. These optical trapping approaches allow for the measurement of weak pico-Newton forces and open new applications [2, 3]. Optical trapping is often described in terms of the gradient force, which pulls the object in the direction of increasing intensity of the focused beam, and the scattering force derived from photon backscattering, that pushes the object along the beam axis. A focused Gaussian beam has light intensity gradients both along the beam axis and perpendicular to it. The resulting optical gradient forces pul the high-index objects towards the focus with the highest intensity, and a stable trapping is achieved when they overcome the scattering and gravity forces. Usually, these objects (such as particles or biological cells) have a material composition and, thus, refractive indices different from that of the surrounding medium, as needed for noncontact manipulation [3].

Applications of laser tweezers in the liquid crystal (LC) research only begin to be explored [6-16]. LCs are usually composed of anisometric molecules, flow like ordinary liquids, but exhibit long range orientational order along with varying degrees of positional order, similar to solid crystals [17,18]. The average local orientation of the LC molecules is described by the director $\hat{N}$ [17]. From the optical standpoint, an aligned LC is a uniaxial monocrystal with an optic axis along $\hat{N}$. Recently, there has been a growing interest to manipulate colloidal particles immersed in LCs [7,8,10-14], defects in Langmuir monolayers [19-24], textures [25], and LC droplets [6,15,16,26-30]. Because of the richness of observed phenomena and fascinating experimental capabilities, optical trapping shows a great promise to become one of the mainstream techniques in the LC studies. For example, both dipolar [8, 10] and quadrupolar [7] colloidal interactions between the particles in nematic LCs have been explored using laser tweezers. Optically trapped particles allowed LC disclinations to be manipulated and their line tension to be measured [10, 13]. Laser trapping of nematic droplets allows one to transfer the optical angular momentum to the droplets and induce their rotation [6, 15, 16, 26, 28].

In this article, we demonstrate laser manipulation of director structures in LCs when no foreign inclusions are present. The studied samples have homogeneous composition, but spatially-varying structures of molecular orientations. Since the LC's effective refractive index depends on the LC director orientation and on the light polarization state, the spatially-localized director structures usually have an effective refractive index different from that of the surrounding LC. This refractive index contrast allows the structures to be manipulated using polarization-controlled optical gradient forces that can be varied from attractive to repulsive. In most of the experiments, the used laser powers are below the threshold for optical Freedericksz transition, when the laser-induced realignment can be neglected. For this regime, extending the approach of Tlusty *et al*. [31], we calculate the optical gradient forces for typical director structures and find a fair agreement with the experiments. Optical trapping properties at high laser powers are modified by the laser-induced changes of the refractive index pattern and, thus, the modified optical gradient forces. In addition, elastic interactions between the laser-induced director distortion and the structure give rise to elastic forces comparable with the optical forces. We also show that polarized high-power beams allow one to exert torsion on LC disclinations. Optical manipulation of the director structures is important for fundamental LC research and for applications in displays, telecommunications, spatial light modulators, tunable photonic crystals, and artificial negative-index materials.

2. Experimental techniques and materials

For optical manipulation, we used a trapping system consisting of an optical manipulator (Solar-TII, LM-2), a TEM_{00} CW Nd: YAG laser (COHERENT, Compass 1064-2000), and a microscope (NIKON, TE-200) [10]. An optical trap was formed using an immersion oil 100× objective (numerical aperture NA=1.3) with ~60% transmission at $1064nm$. The focused beam

#78218 - $15.00 USD Received 21 December 2006; revised 25 February 2007; accepted 26 February 2007

was steered in the horizontal plane by a computer-controlled galvano-mirror pair and visualized by a co-localized low-power ($<100\mu W$) beam of a HeNe laser ($633nm$). The vertical position of the laser trap was controlled by a piezo-stage with $0.1\mu m$ accuracy. Simultaneously with optical trapping, we conducted polarizing microscopy (PM) and bright-field optical microscopy observations using a charge-coupled device (CCD) camera Micropublisher 3.3 RTV (QImaging). Additionally, the vertical cross-sections of some of the cells were visualized using Fluorescence Confocal Polarizing Microscopy (FCPM) [32-35].

LC cells were assembled from plates coated with either polyimide PI2555 (HD MicroSystems) alignment layers buffed to set the uniform in-plane far-field director $\hat{N}_0$, or with the polyimide JALS-204 (JSR, Japan) for homeotropic anchoring (with $\hat{N}_0$ perpendicular to the substrates). The sample thickness $(5-50)\mu m$ was set using strips of mylar films placed along cell edges. After the cell was sealed using a UV-curable glue, the cell gap thickness was measured using the interference method [33, 34]. The samples were prepared using either room-temperature smectic LC 8CB (octylcyanobiphenyl, obtained from Aldrich) or a nematic LC AMLC-0010 (obtained from AlphaMicron Inc.). Refractive indices of AMLC-0010 are the following: ordinary index $n_o = 1.47$; extraordinary index $n_e = 1.55$ [34]. The respective indices of 8CB are $n_o = 1.52$ and $n_e = 1.69$. To obtain the cholesteric LC, AMLC-0010 was doped with a chiral additive ZLI-811 (obtained from EM Industries) with the helical twisting power of $10.47\ \mu m^{-1}$ [34]. By adding different amounts of the chiral agent (up to 10 *wt.*%), the cholesteric pitch was varied within $(1-20)\mu m$. For the FCPM studies, the LCs were doped with ~ 0.01 % of a fluorescent dye N,N'-Bis(2,5-di-tert-butylphenyl)-3,4,9,10-perylenedicarboximide (BTBP). Using a 60× objective (NA=1.4) and the confocal microscope working in the FCPM mode [35], BTBP was excited by an Ar-laser at 488*nm* and fluorescence was detected within the spectral range 510-550*nm*. All used materials are transparent at the trapping wavelength $1064nm$, so that no significant laser-induced sample heating ($>1^0C$) was observed. The LC cells were filled by the capillary forces in the isotropic phase (to avoid any flow influence on the LC alignment) and then cooled down to the room temperature. After the material is brought into the nematic, cholesteric, or smectic phase, the defects and structures spontaneously nucleate; in this work, these director structures are studied from the standpoint of their optical manipulation.

3. Results

3.1 Optical microscopy of director structures

Molecular orientations in LCs form a wealth of complex three-dimensional (3-D) patterns of the director $\hat{N}(\vec{r})$, that depend on the treatment of confining surfaces, presence of inclusions and chiral agents, flow and temperature changes, etc. Figures 1-4 show the typical director structures, which we selected to explore optical trapping properties. The structure shown in Figs. 1(a), 1(d) contains the domain with the uniform $\hat{N}$ and the domain with 180^0-twisted $\hat{N}$ across the cell, separated by a disclination [32]. Cholesteric fingers in a homeotropic cell, Fig. 1(b), contain the local in-plane twist of $\hat{N}$, which is matched to the homeotropic boundary conditions at the substrates by the two twist disclinations, Fig. 1(e) [34]. In the axially-symmetric structure of the toric focal conic domains (TFCDs) in a smectic LC, Figs. 1(c), 1(f), the smectic layers fold around two defect lines, a circle and a straight line passing through the circle's center [35, 36]. $\hat{N}(\vec{r})$ within the TFCD's vertical cross-section is shown in Fig. 1(f).

The cholesteric circular domains (CDs) shown in Fig. 2 are observed in LC cells with homeotropic treatment of the confining substrates and the cell gap approximately equal to the cholesteric pitch *p*. The director structure of the CD is rather complex, but, for simplicity, can be represented as in Fig. 2(f), where $\hat{N}$ is orthogonal to the cell substrates in the center of the

#78218 - $15.00 USD Received 21 December 2006; revised 25 February 2007; accepted 26 February 2007

domain, and twists by 180^0 as one moves to the domain's perimeter in all radial directions. This π-twist of the director matches overall untwisted homeotropic ($\hat{N}$ perpendicular to the cell substrates) director field in the rest of the LC cell.

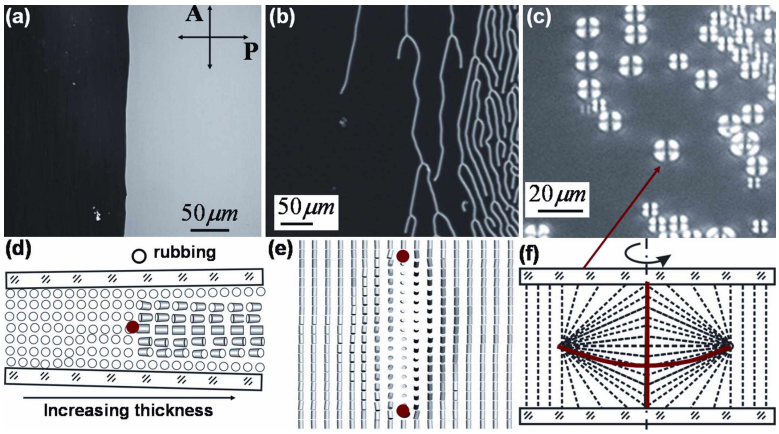

Figs. 1. (a). – 1(c). Polarizing microscopy textures: (a) domains with a uniform (left) and the 180^0-twisted across a cell director (right); (b) cholesteric fingers in a homeotropic cell; (c) toric focal conic domains in a smectic LC. (d-f) Director fields in vertical cross-sections of the structures: (d) for a wedge cell shown in (a) with a disclination line separating the two domains; (e) for a cholesteric finger of the CF3 type; (f) for the toric focal conic domain. The defect lines in (d-f) are marked by the red lines or filled circles. Note that four different types of cholesteric fingers are known [34], and (e) illustrates the simplest one. Crossed polarizers in (a-c) are along the vertical and horizontal image edges.

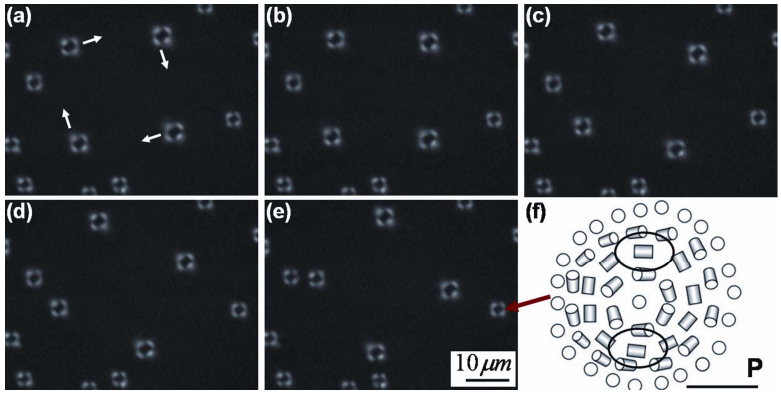

Fig. 2. Optical manipulation of cholesteric CDs: (a, 2 MB) video sequence and (b-e) extracted images. Using a single beam that is time-shared between four traps, four CDs (marked by white arrows in (a)) are first positioned in vertices of a square and then are set to follow computer-programmed concentric motion trajectories as shown in video frames (a-e) taken at about 1s time intervals. (f) The director structure of the CD in the plane of the LC cell. Textures (a-e) were obtained with the crossed polarizer and analyzer along the image edges. The black ellipses in (f) mark the two equally-possible trapping cites for large CDs when the trap's linear polarization is along the horizontal direction (marked by the black bar and "**P**").

Figure 3 shows a dislocation of Burgers vector $b = p$ in the cholesteric layered structure, obtained in a cell with planar boundary conditions and thickness much larger than the pitch. The dislocation core is split into two λ-disclinations of half-integer strength and opposite signs [32, 33]. The director $\hat{N}$ in the center of the escaped λ-disclination is along the defect line, Fig. 3, making it non-singular [32]. Another director structure in the lamellar cholesteric system shown in Fig. 4 contains a quadrupole of the non-singular half-integer λ-disclinations.

#78218 - $15.00 USD Received 21 December 2006; revised 25 February 2007; accepted 26 February 2007

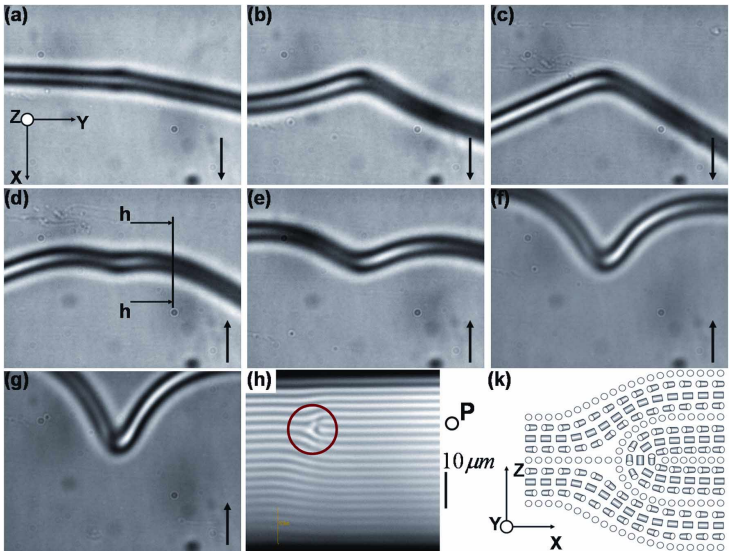

Fig. 3. Stretching of an optically trapped dislocation in a lamellar LC by moving the sample using a stage: (a, 1.1 MB) video sequence and (b-g) extracted representative image frames. The directions of the sample displacement are shown by the black arrows in (a-g). (h) Layers profile in the vertical FCPM cross-section that was obtained (before the optical trapping experiments) in the plane orthogonal to the dislocation, as shown by the h-h line in (d). Schematics of the director field around the defect core shown by the red circle in (h). Linear polarization direction of the trapping laser beam is along the y-axis in (a-g). FCPM polarization direction in (h) is along the defect line. Polarizing microscopy textures (a-g) were obtained with the crossed polarizer and analyzer along the vertical/horizontal image edges.

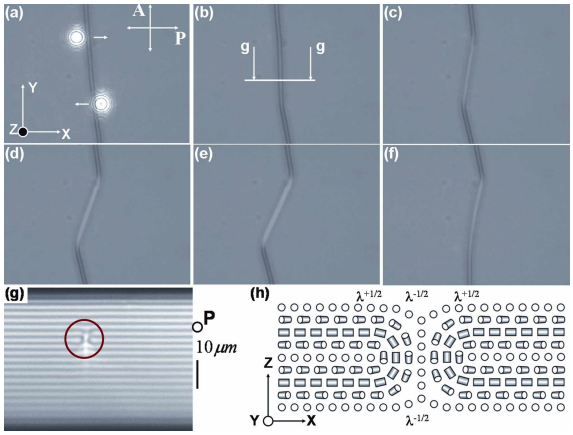

Fig. 4. Laser manipulation of a disclination quadrupole: (a, 1.9 MB) video sequence and (b-f) extracted frames. A single beam is time-shared between the two IR traps visualized in (a) by a HeNe laser beam co-localized with the trapping beam. The traps are slowly shifted as shown by white arrows in (a) and the disclinations are stretched (a-f) until they escape from the traps (f), because of their line tension. (g) Layers structure visualized by the FCPM for the vertical cross-section perpendicular to the cluster, as marked by the g-g line in (b). (h) The director field around the disclination cluster shown by the red circle in (g). Linear polarization of the laser beam used for manipulation is along the y-axis in (a-f). FCPM polarization direction is normal to the image and along the cluster in (g). Textures (a-f) were obtained with the crossed polarizer and analyzer along the image edges.

#78218 - $15.00 USD Received 21 December 2006; revised 25 February 2007; accepted 26 February 2007

3.2 Laser trapping and manipulation with low-intensity beams

Linearly-polarized optical traps can manipulate all structures described above. As an example, we demonstrate laser-controlled transportation of cholesteric CDs along the computer-programmed trajectories using time-shared dynamic laser traps [37], Fig. 2. These structures start to be attracted to the laser trap at distances less than $3\mu m$ from their perimeter. At the used power $8mW$ per one trap, no laser-induced director distortions are observed, Fig. 2. Optical trapping depends on the structure's in-plane size, refractive index distribution, and the beam's polarization state. For example, the CDs much larger than the beam waist are trapped at the two equally-probable high-index regions, where the beam's linear polarization matches the in-plane director, Fig. 2(f); the CDs of radius $2\mu m$ and less are trapped at their center.

The boundary between the untwisted and twisted domains in Figs. 1(a), 1(d) can be displaced along the thickness gradient using a focused laser beam of power $\sim 10mW$. Noticeable interaction of the defect line with the trap starts at a separation distance less than $3\mu m$; the structure remains intact if the focused beam is farther away. When the laser beam is polarized along the rubbing direction, Figs. 1(a), 1(d), the untwisted domain of the structure can be slowly shifted (at $(1-5)\mu m/s$) by the beam in the direction of increasing cell thickness. When the beam's linear polarization is orthogonal to the defect line (along the thickness gradient), one can shift the π-twisted domain into the direction of decreasing thickness of the wedge cell, Fig. 1(a), 1(d). In other words, the untwisted domain is attracted to the laser trap with polarization along the rubbing direction and repelled from the trap polarized along the thickness gradient; the vice versa polarization dependence of the trapping properties is observed for the twisted domain. The linear light polarization does not follow the director twist while the beam is traversing through the sample (cell thickness $\approx 5\mu m$, optical anisotropy $\Delta n \approx 0.08$) [32]. Therefore, the above observations are natural and correspond to attraction of the high-refractive-index LC domains to the laser trap and repulsion of the low-index ones.

Cholesteric fingers, Figs. 1(b), 1(e), are attracted to the laser trap with a linear polarization parallel to their axes starting from distances $(2-3)\mu m$. They can be stretched or continuously shifted when the beam is displaced perpendicular to the finger. Moving the laser trap along the finger leaves the structure intact, unless the trap approaches one of the finger's ends. In the later case, the optical trapping forces cause the finger drift along its axis in the direction of the displacing laser trap. When the beam polarization is orthogonal to a finger, no trapping is observed at powers $< 15mW$, as expected considering that there is no refractive index contrast in this case, Fig. 1(b), 1(e). Manipulation of the axially-symmetric TFCDs [Fig. 1(c), 1(f)] in the matrix of planar smectic layers is direction insensitive. Regardless of the trap's polarization state, the TFCDs always have the effective refractive index higher than that of the surrounding smectic LC with $\hat{N}$ orthogonal to the substrates. Optical trapping is efficient when the beam's focus is in the plane of the TFCD's circular line defect, because of the abrupt change of the director from horizontal (within the domain) to vertical (around it), corresponding to a large refractive index contrast, Fig. 1(f). The index contrast is weaker near the confining plates, Fig. 1(f); therefore, optical trapping is less effective if the laser is focused close to one of the substrates.

Optical manipulation of the director structures shown in Figs. 1 and 2 is two-dimensional, because these structures span across the entire cell gap. The situation is different for dislocations of Burgers vector $b = p$ in the planar system of cholesteric layers, Fig. 3. For a beam with linear polarization along the disclination, the effective refractive index within the structure is close to n_e and larger than that of the surrounding LC. This allows the dislocations to be optically trapped, Fig. 3. The structure is repelled from the beam if its polarization is orthogonal to the disclination, because the refractive index difference between the dislocation and the surrounding LC is negative in this case. Axial optical trapping forces are, in general, weaker than the trapping forces in the lateral plane, but sufficient for

#78218 - $15.00 USD Received 21 December 2006; revised 25 February 2007; accepted 26 February 2007

manipulation. For example, at powers $30mW$ and larger, they allow one to produce dislocation kinks and anti-kinks [32] that mediate dislocation shift across the layers (along the microscope's optical axis), Fig. 3(h). Manipulation of the quadrupole of λ-disclinations, Fig. 4, also employs polarization dependence of the structure's effective refractive index, which can be varied from values smaller to higher than that of the LC around it. Both attractive and repulsive forces can be effectively used for optical manipulation. For example, the director structure in Fig. 4 is repelled from the linearly polarized laser trap with polarization perpendicular to it, but can be stretched and efficiently manipulated using two time-shared laser traps located at the opposite sides of the cluster.

3.3 Optical manipulation using high-intensity beams

Optical trapping with high-intensity focused laser beams is different from that described above. At high powers (usually $\geq (30-45)mW$, depending on the LC and cell thickness), a tightly-focused polarized laser beam [38, 39] locally reorients the director and produces elastic distortions, causing the optical Freedericksz transition [11, 12, 27, 29, 40-43]. This alters the optical trapping properties. For example, at powers $< 40mW$, the cluster shown in Figs. 4 and 5 is repelled from a focused beam with the linear polarization orthogonal to it. At higher powers, this beam locally reorients the director and exerts torsion on the structure, Fig. 5(a), 5(c), so that the disclinations in the cluster are locally parallel to the beam's polarization. The cluster with locally realigned director is then trapped by the beam and can be translated within the sample's plane. In a similar way, a cholesteric finger [Fig. 1(b)] can not be manipulated by a low-intensity beam with polarization perpendicular to the finger, as described above. However, the LC director is locally reoriented and trapping becomes possible at high powers; the focused laser beam causes local reorientation of the finger at powers $> 100mW$, similar to the case of the cluster shown in Fig. 5. Clearly, high-power laser beams allow the director structures to be not only spatially translated but even locally reoriented by changing the focused beam's polarization.

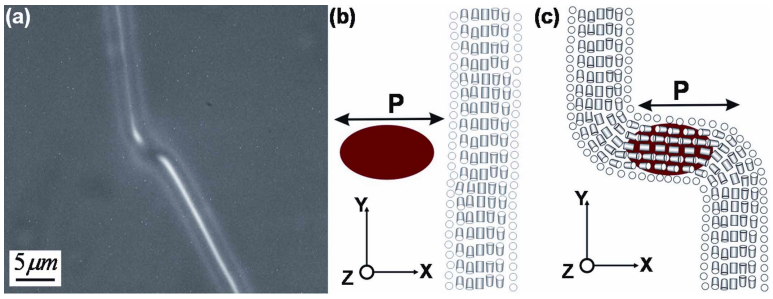

Fig. 5. (a). An image showing that a linearly-polarized beam of power $W \approx 100mW$ exerts torsion and locally reorients an initially straight disclination cluster shown in Figs. 4. (b), 4(c) Schematics of the molecular alignment in the central part of (b) the undistorted cluster [similar to that shown in Fig. 4(h)] and (c) with the local laser-induced director reorientation that results in the structure trapping at high powers, as shown in (a). Crossed polarizers are along the image edges in (a).

4. Discussion

4.1 Refractive index contrast in liquid crystals with spatially-varying director

Polarized laser manipulation of the LC structures, Figs. 1-4, utilizes the spatially-inhomogeneous refractive index patterns. Depending on the local director $\hat{N}$ (optic axis), the effective refractive index n_{eff} can vary from n_o to n_e, which results in the polarization-controlled refractive index contrast between the LC domains. Unlike in the case of colloidal particles suspended in liquids (where the refractive index changes abruptly at the particle-fluid

#78218 - $15.00 USD Received 21 December 2006; revised 25 February 2007; accepted 26 February 2007

interface), the effective refractive index in LCs usually changes on the scale of microns. This is because the abrupt changes of LC director would be costly in terms of the elastic free energy [17, 18]. The exceptions are the structures containing defects with a singular core (such as point defects, line defects, and defect walls), at which the LC domains with strongly misaligned $\hat{N}$ are joined, Fig. 1. These defects usually have the size of a core with undefined $\hat{N}$ in the $(10-100)nm$ range [17, 18]; from an optical standpoint, this corresponds to instant spatial changes of $\hat{N}$ and of the effective refractive index. For example, the in-plane orientation of $\hat{N}$ jumps by 90^0 at the disclination separating the uniform and twisted domains in the wedge cell [Fig. 1(d)] and at the circular defect line of the TFCD [Fig. 1(f)] separating the regions with $\hat{N}$ orthogonal (outside the domain) and parallel (within the TFCD) to the bounding plates. Respectively, the local effective refractive index at the defect lines can jump between n_o and n_e or can be varied within some fraction of optical anisotropy $\Delta n = n_e - n_o$, depending on the beam's polarization and the actual $\hat{N}(\vec{r})$.

4.2 Optical gradient forces

Modeling of optical trapping of the director structures requires the knowledge of the 3-D refractive index patterns, which can be calculated only for known $\hat{N}(\vec{r})$. However, analytical expressions for $\hat{N}(\vec{r})$ of the localized structures are often not available. To get qualitative insights into the optical trapping properties of the director structures, we model them as dielectric objects with an effective refractive index n_{DS} and shape mimicking that of the structure, Fig. 6, surrounded by the LC with an effective index n_{SLC}. The simple models in Figs. 6(a)-6(c) correspond to director structures such as those shown in Figs. 1(d)-1(f). We calculate the optical gradient force exerted by a tightly focused beam on a director structure using the approach of Tlusty *et al.* [31]. This approach was already successfully applied for complex anisotropic systems such as LC droplets and colloidal particles in LCs [14, 26]. The interaction energy between the laser trap and the structure reads:

$$f(r) = \frac{\varepsilon_0}{2}[n_{SLC}^2 - n_{DS}^2] \int_{V_{DS}} \vec{E}(r,z)^2 dV, \tag{1}$$

where $\vec{E}(r,z)$ is the electric field of the tightly focused laser beam, ε_0 is vacuum permittivity, and integration is performed over an effective volume of the director structure V_{DS}. In general, one would need to consider the actual electric field distribution in a tightly-focused laser beam [38, 39] and account for aberrations due to focusing through dielectric interfaces, defocusing in the birefringent medium, as well as the change of the beam's polarization state while traversing the LC. However, the resulting beam intensity distribution is complex. Instead, to obtain a qualitative insight, we follow Ref. [31] and assume that the optical trap is formed by an axially-symmetric three-dimensional Gaussian beam. We then perform integration in Eq.(1) and calculate the trapping force $\vec{F}(r) = -\nabla f(r)$ in the lateral plane perpendicular to the beam axis $\hat{z}$ for typical shapes of director structures, Fig. 6.

For the structure modeled as in Fig. 6(c) with $l_x = l_y = l_z = l$ (a cubic domain), the optical gradient force at distances r from the trap center reads:

$$F^{cubic}(r) = A^{cubic} \exp[-\frac{r(l+r)}{2\omega^2}][\exp(\frac{lr}{\omega^2}) - 1], \tag{2}$$

where

$$A^{cubic} = \frac{2g\xi W(n_{DS}^2/n_{SLC}^2 - 1)}{c} erf(\frac{l}{2\sqrt{2}\omega}) erf(\frac{l}{2\sqrt{2}\omega\xi}) \exp(\frac{-l^2}{8\omega^2}), \tag{3}$$

#78218 - $15.00 USD Received 21 December 2006; revised 25 February 2007; accepted 26 February 2007

c is the speed of light, ω is the size of the beam waist, W is the laser power, g is a coefficient of the order of unity that depends on the LC refractive indices, and ξ is the ratio between the focused beam size along $\hat{z}$ and perpendicular to it [31]. Equations (2) and (3) explain the attraction of the director structure to the trap for $n_{DS} > n_{SLC}$ and repulsion at $n_{DS} < n_{SLC}$. With increasing the center-to-center distances r between the beam and the structure, the force linearly increases at small r, is maximum when the beam is close to the structure's edge ($r \approx \pm l/2$), and decreases at larger r. When the structure is much larger than the beam's waist, $l >> \omega$, the gradient force is strong only at the structures' edges ($r \approx \pm l/2$), Fig. 6(f), in agreement with the experimental observations.

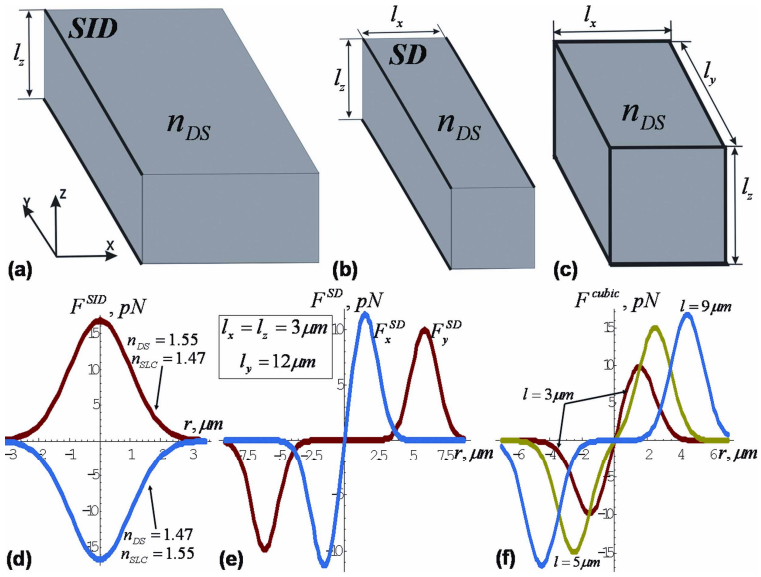

Fig. 6. Models of the LC structures and the calculated optical gradient forces. (a) A semi-infinite domain (SID) of thickness l_z, extending from x=0 (thick lines in (a)) to infinity ∞ along the x-axis and from $-\infty$ to ∞ along the y-axis. (b) A stripe-like domain (SD) of thickness l_z, width l_x, and extending from $-\infty$ to ∞ along the y-axis. (c) A domain with finite dimensions. (d-f) Calculated gradient forces vs. the distance to the trap's center: (d) for the structures shown in (a) using Eq.(6); (e) for the SD fragment using Eq.(4) and sizes marked on the figure; (f) for the structure shown in (c) using Eq.(2) and the marked sizes $l = l_x = l_y = l_z$. We used $W = 15mW$ and indices marked in (d) in calculations for the SID. Indices $n_{DS} = 1.55$, $n_{SLC} = 1.47$ were used in the calculations for the SD and the cubic domain in (e,f).

Optical gradient forces acting on anisotropic structures [Figs. 6(a), 6(b)] are direction-sensitive. For the stripe-like domains (SDs) with dimensions $l_x = l_z = l$ and $l_y >> l >> \omega$, the forces in the beam's lateral plane are different when measured in the directions along (y) and perpendicular (x) to the elongated structures (Fig. 6):

$$F_{x/y}^{SD}(r) = A_{x/y}^{SD} \exp[-\frac{r(r+l_{x/y})}{2\omega^2}][\exp(\frac{rl_{x/y}}{\omega^2})-1], \quad (4)$$

where

#78218 - $15.00 USD Received 21 December 2006; revised 25 February 2007; accepted 26 February 2007

$$A_{x/y}^{SD} = \frac{2g\xi W(n_{DS}^2/n_{SLC}^2-1)}{c} erf[\frac{l_{y/x}}{2\sqrt{2}\omega}] erf[\frac{l_z}{2\sqrt{2}\omega\xi}] \exp[\frac{-l_{x/y}^2}{8\omega^2}]. \quad (5)$$

The anisotropy of the trapping forces is natural as the SDs are anisometric objects [14]. For SDs with $l_x = l_z = l$ and $l_y \to \infty$, the forces along the stripes (y-direction) vanish, $F_y^{SD} = 0$, in agreement with the experiments. The force $F_y^{SD}(r)$ acting on the SD fragments of length much larger than their width ($l_y >> l_x >> \omega$) is strong only at the SD's ends. This explains the experimental observation that the SD fragment (such a cholesteric finger) remains intact when the laser trap is displaced along its axis, unless the beam approaches one of its ends.

The optical gradient force acting on the semi-infinite domains [SIDs, Figs. 6(a), 6(d)] reads:

$$F_x^{SID}(r) = \frac{2g\xi W(n_{DS}^2/n_{SLC}^2-1)}{c} \exp(-\frac{r^2}{2\omega^2}); F_y^{SID} = 0. \quad (6)$$

In agreement with the experimental observations for a similar structure [Figs. 1(a), 1(d)], no force is exerted when the trap is displaced parallel to the boundary between the two domains, $F_y^{SID} = 0$. Equation (6) shows that a focused beam can pull the high-index director structure towards the low-index LC domain when the optical trap is shifted perpendicular to the domain boundary, Fig. 6(d), as observed experimentally. For the SIDs [such as in Fig. 1(a)] the trapping force can be varied in a broad range, as both n_{DS} and n_{SLC} can be varied from n_o to n_e by changing beam polarization [Fig. 6(d)]. Optical forces calculated using Eq. (6) are noticeably strong only when the beam is at distances $2\mu m$ or less from the domain interface [Fig. 6(d)], as in the experiments.

To calculate the optical gradient forces acting on cholesteric CDs, we represent the director in the cylindrical coordinate system: $\hat{N}_{CD} = (0, \sin(2\pi \cdot r/p), \cos(2\pi \cdot r/p))$ for distances $< p/2$ from the CD's center and $\hat{N} = (0,0,1)$ at distances $\geq p/2$. We first calculate the spatial refractive index distribution for this director field and then obtain numerical results for the optical gradient forces, Fig. 7, employing the same approach as used above. Interestingly, when the in-plane size of the CD becomes much larger than that of the focused laser beam, the CDs are not trapped at their center any more, Fig. 7, but at the high-index parts of the CD's ring with the in-plane director, as also observed in the experiments [Fig. 2(f)]. In contrast, relatively small CDs of size comparable or smaller than the beam waist are trapped at their center. These results qualitatively agree with the experiments and demonstrate the importance of accounting for the exact spatial distribution of effective refractive index within the director structure, especially when the structure's dimensions are larger than the waist of the focused trapping beam.

Optical forces can be estimated from the balance of the trapping force and the tension of line defects when they are stretched [10]. Using the literature estimates for the line tension of the cholesteric dislocations and disclination clusters [32], we find that the maximum optical trapping force acting on the structures in Figs. 3 and 4 is within $(5-20)pN$ at $W = 15mW$, as obtained in calculations [Fig. 6(e)]. We note, however, that the above modeling of optical forces adopts many assumptions and can describe the trapping properties only qualitatively. To improve the model, one additionally needs to account for the optical scattering forces [39], the actual refractive index patterns, and the exact intensity distribution of the trapping beam [38, 39]. We also note that several trapping artifacts can be caused by the LC's optical properties [17]: (1) strong light scattering due to the director fluctuations; (2) light splitting into ordinary and extraordinary waves traveling with different speeds; (3) change of the beam's polarization state while traversing the LC; (4) when the director is twisted with the helical axis parallel to the beam, its polarization can follow the director twist (Mauguin

#78218 - $15.00 USD Received 21 December 2006; revised 25 February 2007; accepted 26 February 2007

regime). Therefore, the laser trapping of director structures can be very complex and hard to describe analytically, especially in the LCs of strong optical anisotropy and at large depths of optical trapping.

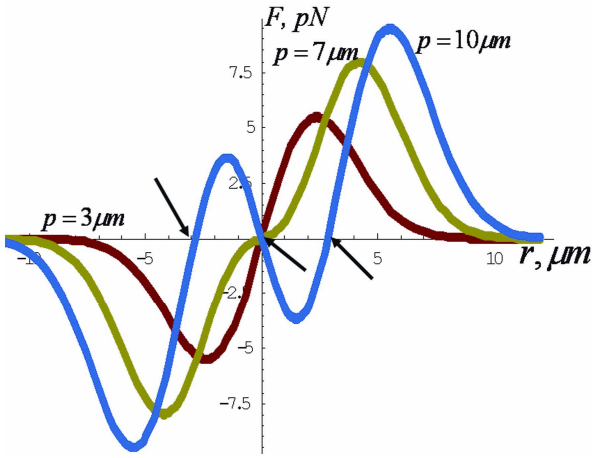

Fig. 7. Optical gradient forces calculated for the cholesteric CD and for power $W = 15mW$. The values of pitch p are marked for each curve. The trapping positions (zero force) are shown by the arrows. Note that large CDs can be trapped at a finite distance from their center.

4.3 Optical manipulation assisted with the laser-induced director distortions

A laser beam of power exceeding the threshold W_{th} locally distorts the director $\hat{N}$ [40-43] and changes the refractive index pattern, which then alters the optical gradient forces, Fig. 5. The maximum laser-induced change of local effective refractive index associated with the director realignment is $\Delta n = n_e - n_o$, which is sufficient to alter the optical trapping properties. The laser-modified pattern of an effective refractive index can be controlled by changing the polarization and power of the trapping beam, allowing one to further tune the optical trapping properties. In addition, laser trapping is modified by elastic structural forces between the structure and the laser-induced distortions, tending to minimize the elastic free energy

$$f_{elastic}(\vec{r}) = \frac{1}{2}\int\left[K_1(\nabla\cdot\hat{N}(\vec{r}))^2 + K_2(\hat{N}(\vec{r})\cdot(\nabla\times\hat{N}(\vec{r})))^2 + K_3(\hat{N}(\vec{r})\times(\nabla\times\hat{N}(\vec{r})))^2\right]dV, \quad (7)$$

where $\hat{N}(\vec{r})$ comprises the structure and the laser-induced director distortions, K_1, K_2, and K_3 are Frank elastic constants for splay, twist, and bend deformations of $\hat{N}$ [17], respectively, and integration is performed over the entire sample's volume. Since the LC elastic constants are typically $\sim 10pN$ [17, 18], one can expect the elastic forces within $(1-100)pN$, comparable to the optical gradient forces at high powers. Manipulation by high-power focused laser beams is, thus, mediated by a combination of both optical gradient forces arising due to the laser-modified refractive index patterns and the elastic structural forces.

The opto-elastic trapping mediated by the director realignment is especially useful for manipulation of the structures with weak refractive index contrast spanning over large distances, which can not be effectively manipulated solely by optical forces at low laser powers. Moreover, the laser-induced realignment allows one to exert torsion and locally reorient disclinations and structures, Fig. 5, which is not possible at small laser powers $< W_{th}$. On the other hand, this realignment can affect quantitative measurements in LCs if it is not accounted for. W_{th} can be controlled by the LC material properties and needs to be established in each experiment. In homeotropic cells [Figs. 1(b) and 2], $W_{th} \propto K_3/(n_e^2 - n_o^2)$ increases with

#78218 - $15.00 USD Received 21 December 2006; revised 25 February 2007; accepted 26 February 2007

decreasing optical anisotropy and/or increasing the bend elastic constant K_3 [40]. In planar cells (Figs.1(a), 3, 4, 5), W_{th} tends to be larger because of the LC's effect on the beam polarization [34, 41]. W_{th} depends on the cell thickness h and the beam waist ω, is larger for $\omega/h << 1$ than for $\omega/h >> 1$ [41, 42], and can be within (10-300)*mW*, depending on the used trapping beams and LC cells. Finally, at very high powers (typically >500*mW*, depending on the LC's absorption at the trapping wavelength), the laser-induced heating may play an important role, even if the LC's absorption is low. In addition to the known effects in isotropic fluids [44], laser-induced heating in LCs may also change the order parameter, or even cause phase transitions, and, thus, can further complicate the interactions between the focused laser beam and the LC structures.

5. Conclusion

We have demonstrated optical trapping of director structures in liquid crystals. At low laser powers, this trapping is mediated by the optical gradient forces exerted by a focused beam on the structures with spatially-varying molecular orientations. The refractive index contrast in the polarized-state laser trapping originates solely from the patterns of molecular orientation. The calculated optical gradient forces reproduce experimental observations for typical structures. When a high-power beam causes director distortions, the trapping properties become qualitatively different for two reasons: (1) the laser-induced director reorientation modifies the refractive index pattern and, thus, the optical gradient forces; (2) the elastic structural forces arise to minimize the distortions in the elastic LC medium. Unlike in the case of particles, gravity forces are completely irrelevant even for trapping of large structures, because there are no density gradients; therefore, large structures (tens or hundreds of micrometers) can be manipulated at low powers of the order of 10*mW*. Optical gradient forces should be accounted for when imaging LCs using laser scanning probe techniques such as FCPM [35]: the laser power should be kept below 1*mW* in order to avoid pulling the high-index director structures into the focused beam of a confocal microscope. The described optical and opto-elastic trapping approaches are not restricted to LCs, and are applicable to all anisotropic materials. Potential applications include composite systems in which at least one of the components is anisotropic, such as polymer dispersed and polymer stabilized LCs.

Acknowledgments

This research was supported by the Institute for Complex Adaptive Matter (ICAM), the International Institute for Complex Adaptive Matter (I2CAM), and by the Directorate of Chemistry and Life Sciences of the Air Force Office of Scientific Research. We thank AlphaMicron Inc. for providing AMLC-0010 and M. Kleman, O. Lavrentovich, B. Senyuk, and G. Wong for discussions.

#78218 - $15.00 USD Received 21 December 2006; revised 25 February 2007; accepted 26 February 2007